Poly(propylene) Nanocomposites Containing Various Carbon Nanostructures

Yunfeng Li, Jiahua Zhu, Suying Wei, Jongeun Ryu, Qiang Wang, Luyi Sun, Zhanhu Guo*

PP nanocomposites containing different carbon nanofillers (CNTs, CNFs, GnPs, CB) are fabricated and further processed by hot compression molding. A high level of nanofiller dispersion is found. The NCs exhibit improved thermal stability and higher crystallinity. Both electrical conductivity and real permittivity increase with increasing nanofiller loading. A strongly aspect ratio dependent electrical conductivity percolation is observed at loadings of 15.0, 12.0, 5.0, and 3.0 wt% for CB, GnPs, CNFs, and CNTs, respectively. The rheological behavior of the NC melts is also investigated. A small concentration of the nanofillers is found to affect the modulus and viscosity of the PP melts significantly.

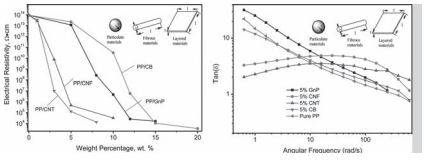

1. Introduction

Conductive polymer composites can be obtained by the combination of an insulating polymer matrix with electrically conductive fillers.[1–10] Among these conductive fillers, carbon-based materials such as carbon black (CB),[11–13] carbon nanotubes (CNTs),[5,14–21] carbon nanofibers (CNFs),[6,8,10,22] graphite powder, and graphene nanoplatelets (GnPs),[2,3,7,23–26] have been used extensively because of their wide availability, low density, high electrical conductivity, and resistance to corrosion. Isotactic poly(propylene) (PP) is one of the most widely used commodity thermoplastics. PP has been widely used in the household appliances, food packaging, automotive components, and medical devices. PP polymer nanocomposites (PNCs) have been extensively investigated over a wide range of applications during the past few decades.[2,6,27–32] In particular, significant property enhancements were reported when carbon nanofillers were incorporated into PP.[2,5,27,32–37]

Carbon is a versatile element. Carbon atoms are capable of bonding with other atoms in sp, sp^2, and sp^3 hybridized structures, generating numerous stable molecules.[38] Thus, carbon has a number of distinct molecular or crystalline forms termed allotropes or polymorphs, which include graphite, diamond, and the more recently discovered fullerenes and graphenes. It can also be shaped into different morphologies such as spherical, fibrous, and layered nanosized materials. More importantly, most of these carbon-based materials are electrical conductive and commercially available. These materials have different aspect ratios and specific surface areas. Figure 1 illustrates the typical carbon nanofillers with different geometries showing different surface area/volume relations. Carbon black, normally a solid composed of spherical particles with diameters from a few tens to hundreds of nanometers, has been one of the most widely used conductive fillers because of its predominant electrical property, low cost, and abundance. However, the low aspect ratio of CB nanoparticle structure leads to high percolation in the PNCs, typically ca. 20 wt% or higher

Y. Li, J. Zhu, Z. Guo
Integrated Composites Laboratory (ICL), Dan F. Smith Department of Chemical Engineering, Lamar University, Beaumont, TX 77710, USA
E-mail: zhanhu.guo@lamar.edu
Y. Li, S. Wei
Department of Chemistry and Biochemistry, Lamar University, Beaumont, TX 77710, USA
J. Ryu
Department of Mechanical & Aerospace Engineering, University of California Los Angeles, Los Angeles, CA 90095, USA
Q. Wang
Department of Chemistry, University of Oxford, Mansfield Road, Oxford, OX1 3TA, United Kingdom
L. Sun
Department of Chemistry and Biochemistry, Texas State University-San Marcos, San Macros, TX 78666, USA

DOI: 10.1002/macp.201100364

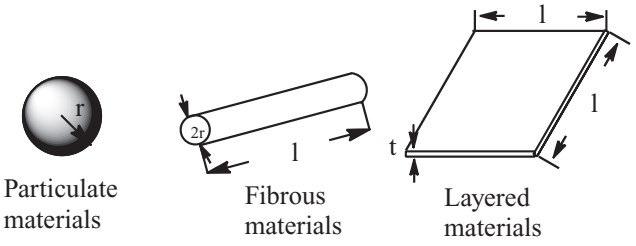

Figure 1. Typical carbon nanofillers with different geometries.

for different insulating polymer matrices.[3,13,39] Although increasing the concentration of CB in the PNCs can enhance the electrical conductivity (σ) and melt viscosity, it also compromises some other physical properties such as mechanical property and hardness.[40–43] On the other hand, both CNFs and CNTs are known to have high aspect ratio (several hundred to thousand), outstanding electrical and mechanical properties with fibrous structure,[10,37,44] Figure 1. Also, GnPs with layered structure have a high aspect ratio together with similar electrical and mechanical properties as those of CNFs and CNTs.[27,45] These fibrous and layered carbon nanomaterials are being widely used to reinforce polymers for improving electrical properties, thermal conductivity, and mechanical properties. PNCs with these carbon nanofillers normally have an electrical percolation threshold between 3 and 10 wt% or even lower.[6,27,45]

The σ of the PNCs can be increased with increasing the conductive filler loading.[6,13,20,25,46] The critical content of the conductive fillers making insulator–conductor transition and forming continuous conducting paths is called percolation threshold. More importantly, a morphological characteristic that is of fundamental importance in the understanding of the structure-property relationship of PNCs is the surface area/volume ratio of the reinforcing materials. As CB, CNFs, CNTs, and graphenes have different geometries, aspect ratios, and physical properties, their effects on the PNC properties should be different. Up to date, there has few reports to compare and analyze the properties of the PNCs derived from their different structures and properties.[37,47]

In this paper, PP PNCs reinforced with various carbon nanostructures were prepared via a facile solvent dispersion strategy. The values of σ of the PNCs with different carbon nanofillers were measured and discussed by weight percentage, volume percentage, specific area, and aspect ratio. The dielectric property of the PP PNCs in the same weight percentage was compared and discussed as well. The effects of the carbon nanofiller types on the thermal stability, crystallinity, and rheological behavior of the PNCs were investigated and discussed in details.

2. Experimental Section

2.1. Materials

The isotactic PP used for this study was supplied by Total Petrochemicals USA, Inc ($\rho = 0.9$ g cm^{-3}, $\overline{M}_n \approx 40\,500$, $\overline{M}_w \approx 155\,000$, melt index: ≈35 g min^{-1}). GnPs were produced by Angstron Materials, Inc. (grade N008-100-P-40) and used as received. The thickness of the platelets (*Z* direction) was 50–100 nm and the average lengths (*X* and *Y* directions) were in the range of 40–50 μm. Vapor-grown CNFs were manufactured by Pyrograf Products, Inc. (CNFs, grade PR-24-XT-LHT), showing high σ. The CNFs are reported to have an average diameter of 100 nm, lengths of ≈50–200 μm, and a density of 1.95 g cm^{-3}. Multi-Walled CNTs (MWCNTs) were supplied from SouthWest NanoTechnologies, Inc. (grade SMW 100) with a diameter of 6–9 nm and purity of ca. 98%. The number of walls is typically from 3 to 6. Spherical super active CB nanoparticles were purchased from Skyspring Nanomaterials with a particle size of around 100 nm and a specific surface area of 1300 m^2 g^{-1}. Details of the carbon nanofillers are shown in Table 1. The solvent xylene (XX0060-3, maximum residue after evaporation: 0.002%, maximum amount of water: 0.05%) with a boiling temperature ranging from 137 to 145 °C was obtained from EM Industries, Inc.

2.2. Preparation of PP/Carbon PNCs

PP and xylene were charged into a flask. The weight ratio of PP and xylene is 1:10, and the weight percentage of the carbon nanomaterials in PP based on the weight of carbon nanofillers to the sum of PP and fillers is adjusted from 1.0 to 20.0 wt%. The corresponding volumetric loading can be determined by the density of the carbon nanofillers and PP.[6]

The PP/xylene mixture was heated and magnetically stirred to around 70 °C for 2 h. A transparent viscous solution was obtained after PP was dissolved completely in xylene. The viscous solution

Table 1. Specifications of different carbon nanofillers.

Material	Density [g cm^{-3}]	Specific area [m^2 g^{-1}]	Length [μm]	Average diameter or thickness [nm]	Aspect ratio
active CB	1.8	1300	≈0.1	<100	≈1
CNTs	2.1	250	>1	≈6–9	120–200
CNFs	1.95	43	≈2	100	100–150
GnPs	2.24	120–150	<50	<100	≈500

was mixed with a predetermined amount of carbon nanofillers, then the above heating and stirring process was repeated overnight. However, the agglomeration of the carbon nanofillers would form if the stirring stops. To avoid agglomeration, the mixture was instantly added into low-temperature deionized water to immobilize carbon nanofillers immediately following the heating process. Afterward, the solidified organic phase system was evaporated at room temperature in the fume hood for 48 h to eliminate xylene. The resulting PP PNCs were used to make discs using a 25 mm diameter mold on a hot press machine heated to 182 °C. These discs were stored in a vacuum chamber for further studies. The main experimental set-ups and the procedures for the nanocomposite preparation were depicted somewhere else.[6,27]

2.3. Characterizations

X-ray diffraction (XRD) analysis was performed on a Bruker AXS D8 Discover Focus diffractometer. The characterization was carried out using a diffractometer with general area detector diffraction system operating with a Cu K_α radiation source filtered with a graphite monochromator ($\lambda = 1.5406$ Å).

The morphology and microstructures of the neat PP and PP nanocomposites were imaged using a field emission scanning electron microscope (FESEM, JEOL JSM-6700F). All disc samples were dipped into liquid nitrogen and fractured. The fractured surfaces were sputter coated with gold to prevent changing and to improve imaging.

To study the thermal stability and crystallization behavior of neat PP and its PNCs, both thermal gravimetric analysis (TGA) and differential scanning calorimetric (DSC) were performed. The TGA experiments were carried out using a TA Instruments Q500 analyzer under a heating rate 10 °C min^{-1} and an air flow rate of 60 mL min^{-1} from 25 to 800 °C. A TA Instruments Q2000 differential scanning calorimeter was used to obtain DSC thermograms. Experiments were run on the samples of about 8–10 mg. Each sample was first heated from room temperature to 200 °C with a heating rate of 10 °C min^{-1} to remove thermal history, followed by cooling down to 40 °C at a rate of 10 °C min^{-1} to record recrystallization temperature, and then reheat to 200 °C at the same rate to determine the melt temperature. The experiments were carried out under a nitrogen purge (50 mL min^{-1}).

The volume resistance (R_v) of the samples was measured by an Agilent 4339B high resistance meter after obtaining the thickness of these composite pellets. The voltage and current limits were set at 1.0 V and 5.0 mA for all the samples. Agilent E4980A Precision LCR Meter (20 Hz to 2 MHz) with signal voltage range of 0–2.0 V_{rms} and signal current range of 0–20.0 mA_{rms} was used to collect the dielectric data at room temperature. The frequency range in the measurement was 500 to 2 MHz.

The rheological behaviors of the neat PP and PP nanocomposite melts were studied by a TA Instruments AR 2000ex Rheometer. The frequency sweep was from 100 to 0.1 rad s^{-1} and the temperature was set at 200 °C when the PP and PNCs were in melt states. The measurements were performed in an ETC Steel parallel plate (25 mm diameter of upper geometry) under nitrogen with 20% strain, which was checked to be in the linear viscoelastic region (i.e., stress and strain were related linearly.)

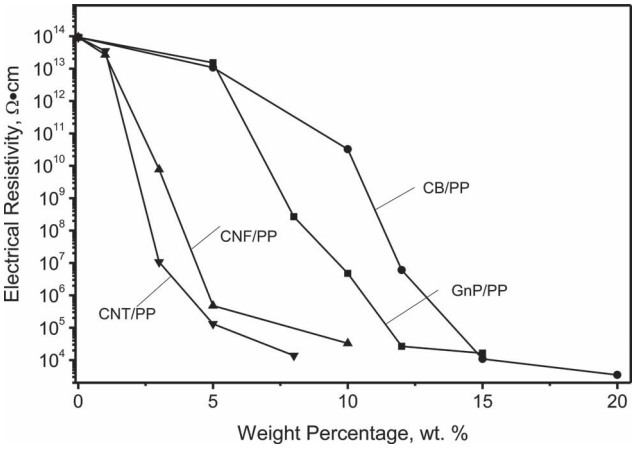

Figure 2. Volume resistivity of the PP PNCs filled with different carbon nanostructures as a function of carbon nanofiller loading.

3. Results and Discussion

3.1. Electrical and Dielectric Properties of the PP Nanocomposites

Like other electrically conductive fillers, carbon nanofillers are excellent candidates for preparing electrically conductive PNCs.[2,6,25,33,48,49] The low electrical resistivity of these carbon nanofillers facilitates the significant increase of the σ in the PNCs when a percolation threshold reaches. As for these four different carbon nanofillers incorporated into insulating PP matrix, the σ of the PNCs increased gradually with increasing the filler loading. Figure 2 presents the electrical resistivity of neat PP and its PNCs with various carbon nanofillers. As compared to neat PP, a slight decrease in the volume resistivity was observed in the PNCs at lower nanofiller loadings. Increased filler loading lowered the volume resistivity. When the nanofiller concentration reached their corresponding percolation thresholds, the PNCs began to convert from an insulator to a conductor showing a decrease of the resistivity by several orders of magnitude. However, due to the different geometries and microstructures of these carbon nanofillers, their percolation threshold values varied. The percolation threshold values were 3.0, 5.0, 12.0, and 15.0 wt% for the PNCs filled with CNTs, CNFs, GnPs, and CB, respectively. In addition, the resistivity decreased more slowly after reaching the percolation threshold in each PNC system.

According to Balberg,[46] the average interparticle distance can be different in the carbon nanofillers with different aspect ratios. The more spherical-like structure, the larger the interparticle distance will be formed. For the elongated particles, their composites have a very narrow distribution of the distances due to the entangled particles structures,[46] and the volume resistivity of

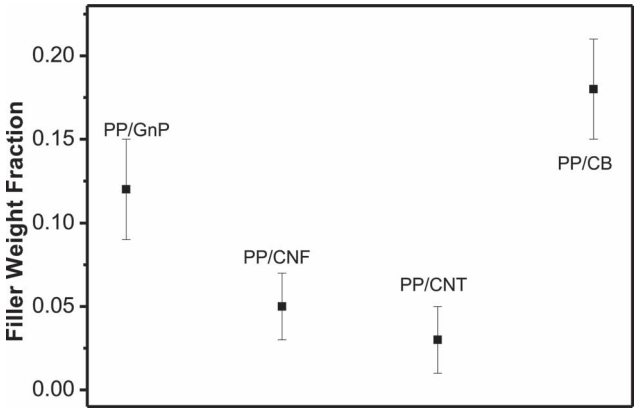

Figure 3. Percolation threshold of the PP PNCs with different carbon materials.

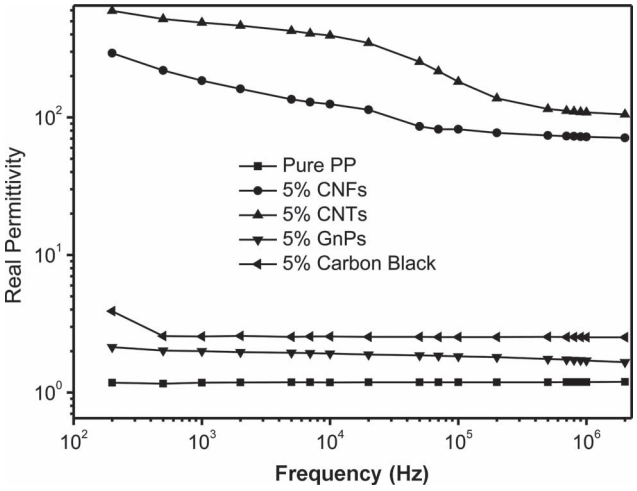

Figure 4. The real permittivity of PP PNCs with a loading of 5.0 wt% different carbon nanostructures vs. frequency at 25 °C.

the composites decreases monotonically with increasing the aspect ratio. As from Table 1, the CNTs and CNFs have much higher aspect ratio than that of the CB nanoparticles. The percolation thresholds of 5.0 wt% for CNFs and of 3.0 wt% for CNTs are much lower than 15.0 wt% for CB in the PP PNCs. Although the GnP itself has higher aspect ratio and a comparable σ than CNFs and CNTs, PP PNCs with GnPs turned to be electrically conductive at around 12.0 wt%. The related results are summarized in Figure 3 for different PNC systems. The agglomeration and curving of the GnPs in PP matrix compromised the effect of high aspect ratio, which was discussed somewhere else.[27] Overall, it shows that the solution strategy is not as effective for the dispersion of GnPs or layer structured fillers as for the fibrous fillers, which is possibly owing to the nature of GnP to easily bend in polymer. Actually, via a solid-state shear pulverization method, a percolation threshold as low as 2.7 wt% was achieved in the PP/exfoliated graphite nanocomposites by Wakabayashi et al.[25] In order to investigate the effects of different carbon nanofillers on the PP PNCs, the same weight percentage (5.0 wt%) was chosen. As depicted in Figure 2, at 5.0 wt%, the volume electrical resistivity for the PNCs with GnPs, CB, CNF, and CNTs is 1.52×10^{13}, 1.02×10^{13}, 4.78×10^{5}, and 1.08×10^{5} Ω cm, respectively.

Various PP PNCs with carbon nanofillers have been investigated for their potential applications in energy storage through measuring their dielectric property.[6,50] Figure 4 depicts the frequency dependent real permittivity (ε') of these PNCs with 5.0 wt% nanofillers at 25 °C. The ε' of neat PP is about 0.2. The ε' of the PP PNCs incorporated with 5.0 wt% of GnPs and CB increased slightly to 1–2. This phenomenon is consistent with the corresponding σ. In addition, for the PNCs with low permittivity, the ε' in PP PNCs is virtually independent of the frequency, indicating a stable dielectric performance of the prepared PNCs upon frequency variation. The PP PNCs containing 5.0 wt% CNFs or CNTs exhibited a huge jump in ε' up to several hundred. Their permittivity gradually decreased with increasing the frequency and stabilized at ca. 100 and 200 for the PNCs with CNF and CNT, respectively, at frequencies higher than 10^6 Hz. The step-like decrease of the ε' toward high frequency is induced by the dielectric relaxation, which suggests that the established percolation network structure is not stable and easily affected by the external frequency disturbances, similar to the poly(vinylidene fluoride)/MWCNTs and elastomer/CNF PNCs.[10,51] The big jump of ε' for the PP PNCs with CNFs and CNTs reveals that the filler network has been formed at 5.0 wt% loading. This result is consistent with the σ, Figure 2. The ε' of the PP PNCs increases with increasing the σ in the entire testing frequency range, which has been reported in PP PNCs reinforced with the CNFs.[6]

3.2. Morphological Characterization

The level of the nanofiller dispersion in the PP matrix primarily determines the nanofiller reinforcing efficiency and the corresponding σ.[34] The morphological characterization is the most important and direct way to evaluate the degree of nanofiller dispersion state. Figure 5A–D shows the representative SEM images of the PP PNCs with 5.0 wt% different carbon nanofillers. For the PP PNCs with CB, Figure 5A, and GnP, Figure 5B, the CB nanoparticles and GnPs can be observed in the PP matrix. However, both CB nanoparticles and GnPs were isolated and formed islands other than the network paths in the matrix. Thus, it is anticipated that both should have low σ in this dispersion state. Moreover, CB particles did not disperse uniformly in the PP matrix and part of them tended to form agglomerates in certain regions, Figure 5A. The spherical geometry determines that the particles are easy to form

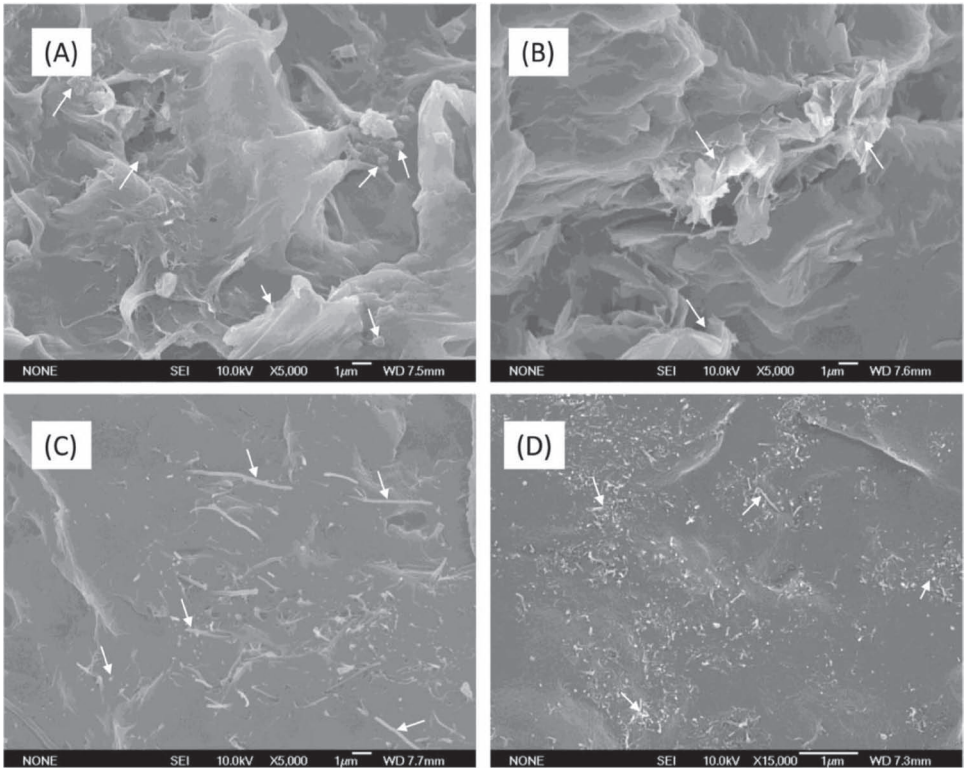

Figure 5. SEM images of the PP PNCs reinforced with (A) CB nanoparticles; (B) GnPs; (C) CNFs; and (D) CNTs at a loading of 5 wt%.

agglomerates, resulting in higher electrical percolation.[37] The agglomeration and bending also happened in the GnP system, Figure 5B, which leads to limitedly utilize the high aspect ratio property.

As shown in Figures 5C and 5D, it is clear that the dispersion of CNFs and CNTs in the PP matrix is more uniform. At 5.0 wt% of CNFs and CNTs, the electron conduction path was formed. In certain areas, the CNT clusters appeared and some CNTs were entangled, which are ascribed to the strong intermolecular forces among CNTs and interfacial interactions between the CNTs and the PP matrix.

3.3. XRD

XRD patterns of PP/GnP, PP/CNT, and PP/CNF with different weight percentages are illustrated in Figure 6A–C, respectively. Carbon nanofillers are observed to have negligible effect on the crystalline polymorph of PP. The peaks of 14.2, 17.0, 18.8, 20.0, and 25.4° are (110), (040), (130), (111), and (060) planes of α phase of PP,[52,53] the α-phase (plane 131 and 041) and β-phase (301) are overlapped between 21 and 22°.[52] The XRD patterns of the PNCs are the combination of the ones from their parent matrix and the filler. The two peaks of GnP (26.7 and 54.8°) appear in XRD patterns of the PP/GnP PNCs and their intensity was elevated as increasing the GnP content,[27] shown in Figure 6A. We take the PP/CNT PNCs as another example, the intensity of the peaks associated with CNTs increased when more CNTs were added into the PP matrix, Figure 6B. The XRD pattern of the pristine CNTs shows a wide peak at 25.7° and a little bump at 41.8°, with which the XRD patterns of PP/CNT became broader at this position when the filler loading was increased. Similar results were obtained in case of the PP/CNF PNCs, shown in Figure 6C. According to the Debye –Scherrer equation,[54] The average grain size is normally estimated by calculating from the full width at half maximum (FWHM) at the major peak,

$$L = \frac{K\lambda}{\beta_{1/2}\cos\theta} \quad (1)$$

where K is 0.9 (constant), λ is 1.5148 (radiation wavelength), $\beta_{1/2}$ is the full width half maximum in radians, and θ is the angle at maximum intensity. These broader peaks yield a decreasing of L, which represents the less agglomeration for the CNT and CNF in PP matrix.

3.4. Thermal Properties of PP/Carbon Nanofiller Nanocomposites

The carbon nanofillers dispersed in the PP matrix are expected to change the thermal properties of the hosting PP matrix. Figure 7 shows the TGA thermograms of the different PP PNCs. The weight loss is observed to start after

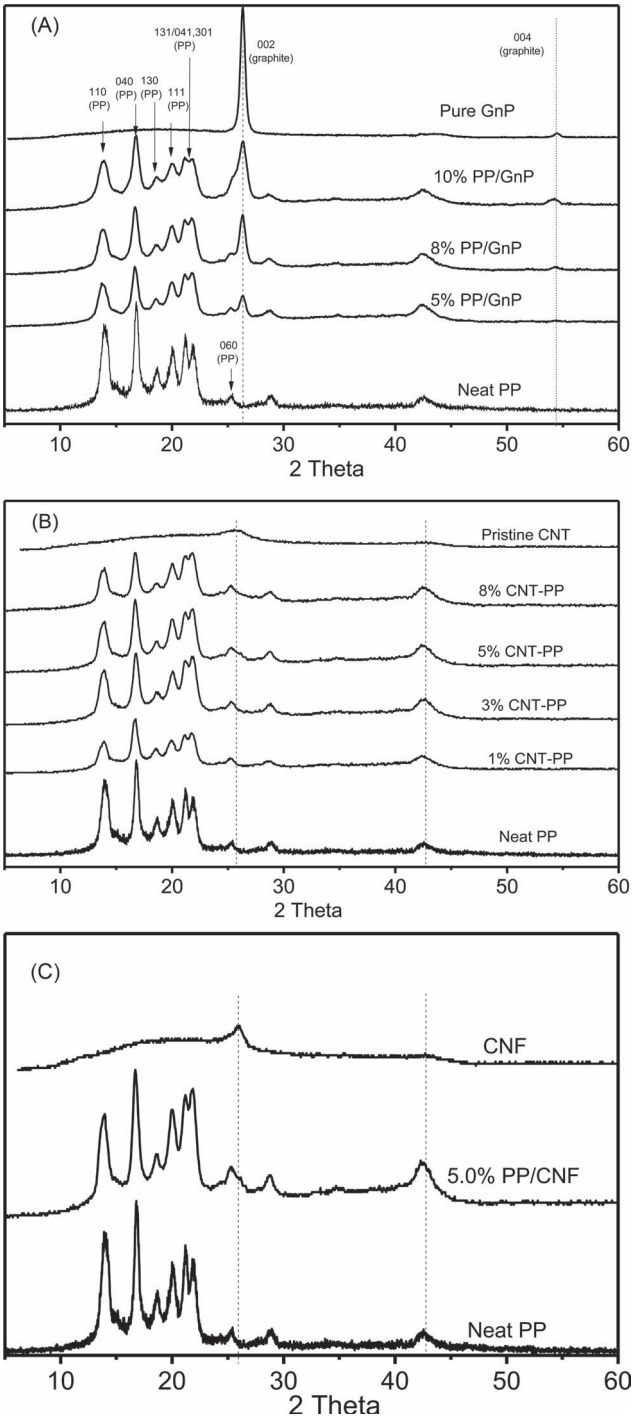

Figure 6. XRD patterns of (A) PP/GnP, (B) PP/CNT, and (C) PP/CNF.

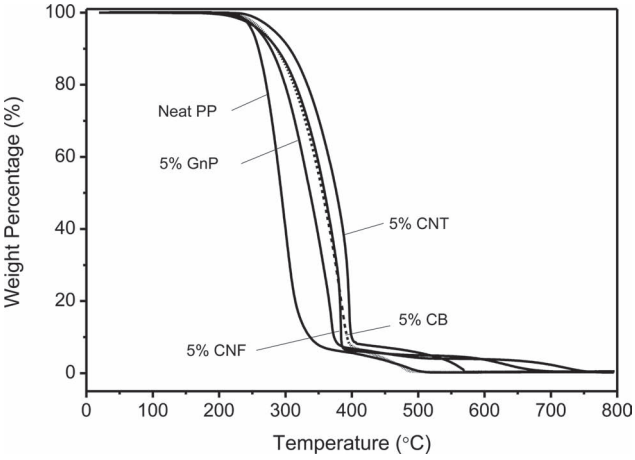

Figure 7. TGA weight loss curves of different PP/carbon nanofiller PNCs with 5.0 wt%.

235 °C for all the samples of the PNCs. The neat PP started to thermally degrade at 220 °C and decomposed completely at 350 °C for pure PP. While all the four PP PNCs exhibited better thermal stability, with ca. 20–45 °C increase in the onset degradation and end-decomposition temperature. The 10 wt% mass loss temperatures ($T_{10\%}$), the temperatures of the maximum rate of the weight loss (inflection point, T_{max}), the end temperatures of the degradation (T_{end}), and the degradation temperature ranges (T_r) are summarized and listed in Table 2. $T_{10\%}$ and T_{max} show that the PP PNCs exhibit an improved thermal stability than that of neat PP. The enhanced thermal stability of the PP/carbon nanofiller PNCs results from the interaction between the PP matrix and the carbon nanofillers. The surface of these carbon nanomaterials absorbs the free radicals produced in the decomposition of PP and restricts the mobility of the polymer molecules.[6,55,56] As CB nanoparticles have much higher specific surface area than the other three, the degradation range is elevated about 10 °C than that of the neat PP. The PNCs with 5.0 wt% CNT appeared to be the most stable than the others, shown in Figure 7. Its $T_{10\%}$ and degradation end are 365 and 407 °C, respectively, improved about 45 °C than those of the pure PP.

The incorporation of different carbon nanofillers was observed to have little effect on the melting temperature (T_m) of PP (about 149 °C), but slightly increased the onset melting temperature (T_{on}) compared to that of neat PP, Figure 8. The T_{on}, T_m, melting enthalpy (ΔH_m), degree of crystallinity (D) and the variation in the degree of crystallinity (ΔD) are summarized and listed in Table 3. The relationship between ΔH_m and D are correlated by

$$D = \frac{\Delta H_m}{\Delta H_o \, f_{PP}} \times 100\% \quad (2)$$

where ΔH_0 is the ΔH_m of the 100% crystalline PP, which is reported to be 209 J g^{-1},[57] and f_{PP} is the PP weight fraction in the PNCs. However, the ΔH_m drastically increased by about 10 J g^{-1} after adding 5 wt% of CNF and CNT, which is much higher than the ones blended with GnPs and CB nanoparticles. The ΔH_m change is an indicator of the variation in ΔD. As summarized in Table 3, PP/CNF and PP/CNT PNCs exhibited a ΔD of 37.5 and 38.6%, respectively,

Table 2. TGA data of pure PP and 5 wt% carbon nanomaterial/PP nanocomposites.

Composite	Temperature of 10% mass loss [°C]	Inflection point [°C]	Degradation end [°C]	Degradation range [°C]
Pure PP	259	312	365	106
5% Graphite	277	340	383	106
5% Active carbon	285	360	400	115
5% CNF	287	360	390	103
5% CNT	305	380	407	102

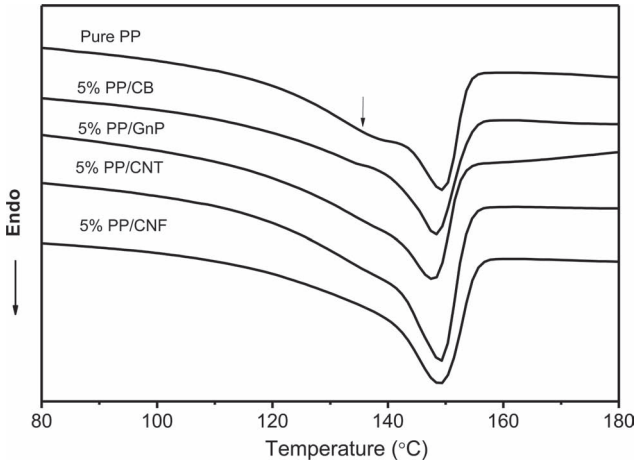

Figure 8. DSC thermograms (second heating cycle) of pure PP and its PNCs compromised with different carbon nanofillers.

representing an increase of 5.4 and 6.6% than that of neat PP. The increased ΔD is owing to the nucleation effect of the CNFs and CNTs.[6,25,27] A similar change of crystallinity after reaching or over electrical percolation threshold was found for the PNCs with higher GnP loading.[27] The fibrous morphology of CNTs and CNFs allows them to effectively serve as nucleating sites in the PP matrix, resulting in a wider exothermic curves and lower recrystallization temperature. In addition, the multimelting behavior of neat PP (as the arrow indicates in Figure 8), which is the visible difference between α and β crystal form,[58] is not obvious or disappeared in the PNCs reinforced with CNT and CNF. This further confirms that the CNTs and CNFs played nucleation sites on the crystallization of PP.

3.5. Melt Rheological Behavior of PP Nanocomposites

The storage modulus (G') in the melt state is a property that is highly sensitive to the formation of a network-like structure in the PNCs. The G' of the PNC melts increases with the addition of GnP loading, especially at low angular frequency (ω). Different from the viscous liquid behavior of the PP melts, a plateau is observed in the low frequency range for the PNC melts, indicating an elastic solid-like behavior. Figure 9A–B depict the G'-ω log–log plot of the PP/CNFs and PP/CNTs PNCs with different weight filler loadings, respectively. Both show a plateau formed at round 5.0 wt%. The G' and G''-ω data for the PNCs with different 5.0 wt% carbon nanofillers are presented in log–log scale in Figure 10A and B. The PP PNCs reinforced with GnPs and CB showed similar behavior to that of pure PP. And the 5.0 wt% PP/GnP PNCs exhibited an even lower G' value than the neat PP, which results from the GnP-PP interlayer slipperiness due to the low surface friction of graphite. These two PNC melts behave like a viscous liquid. However, as discussed above, the 5.0 wt% of PP/CNT and PP/CNF PNCs are electrically conductive and the nanofillers formed a network structure in the PP matrix. Thus, there is a major increase in G' for the PP/CNFs and PP/CNTs PNCs and a plateau is observed at low ω in both cases. The tendency of G''

Table 3. Data of DSC (second heating cycle) of neat PP and 5 wt% PP/carbon nanofiller PNCs.

Composite	Onset melting temperature (T_{on}) [°C]	Melting temperature (T_m) [°C]	Melting enthalpy (ΔH_m) [J g^{-1}]	Crystallinity degree (D) [%]	Variation in the crystallinity degree (ΔD) [%]
pure PP	136.4	149.4	66.28	32.07	–
5% graphite	139.3	147.3	66.75	33.62	1.55
5% active carbon	139.4	148.0	66.19	33.34	1.27
5% CNF	140.4	148.1	74.36	37.45	5.38
5% CNT	141.1	148.2	76.69	38.63	6.56

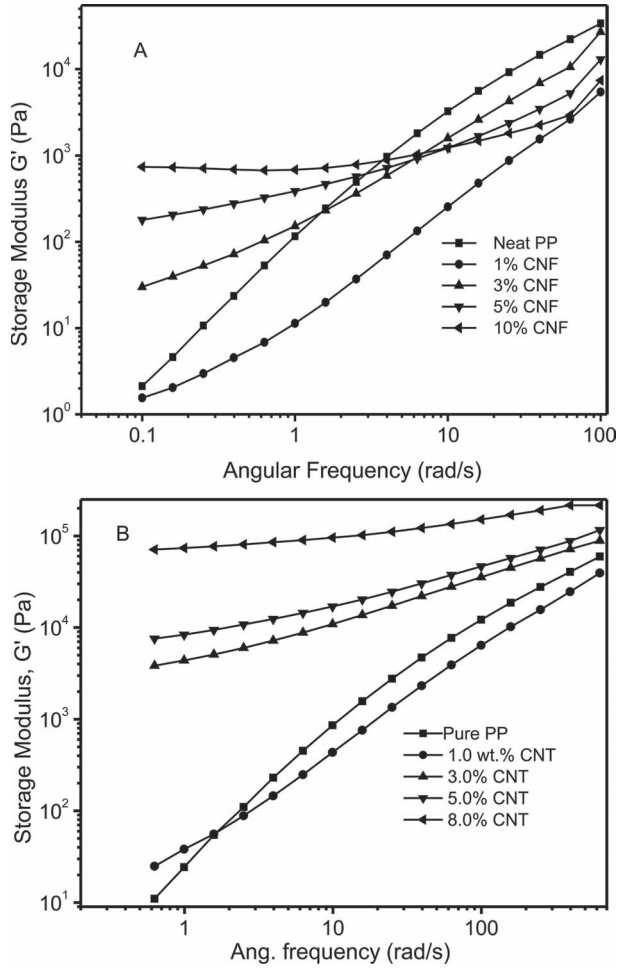

Figure 9. The storage modulus/frequency plot under different CNF and CNT loading. A: PP/CNFs; B: PP/CNTs.

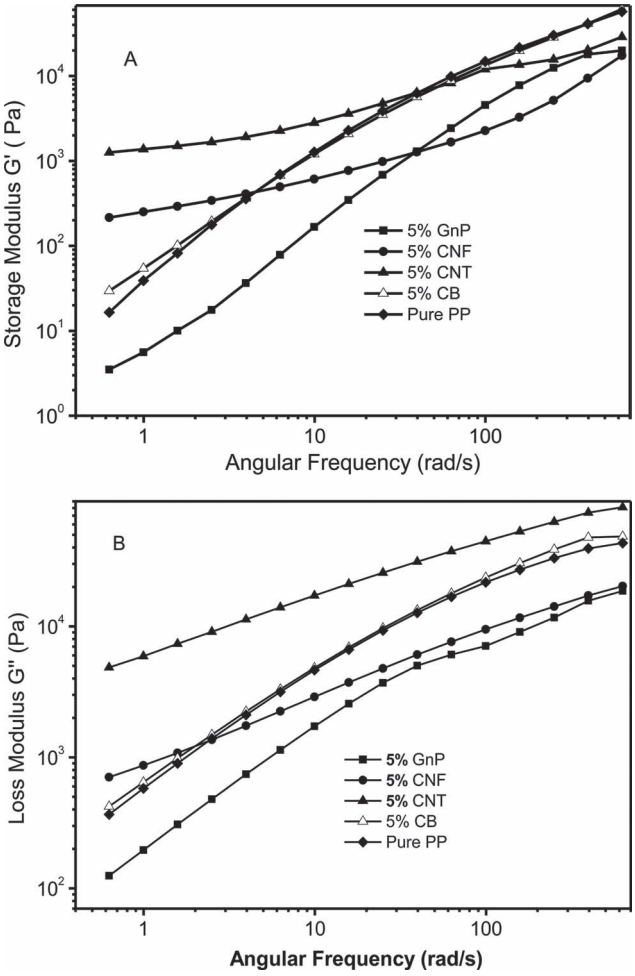

Figure 10. (A) storage modulus (G') and (B) loss modulus (G'') versus angular frequency (ω) for neat PP and its nanocomposites with different carbon nanofillers.

of the PP/CNFs and PP/CNTs PNCs is also different from that of the pure PP, PP/GnPs, and PP/CB PNCs at low ω.

Figure 11 shows the mechanical loss factor (tan δ) as a function of ω. The tan δ, which is the ratio of G'' to G', is highly related to the applied ω. When scanning the experimental ω from low to high frequency, the tanδ of the PNC melts shows three different stages: rubbery, viscoelastic, and glassy state.[6] The tan δ is very low at the rubbery and glassy stages, but it is high at a ω between these two extreme cases. Neat PP and its PNCs with 5.0 wt% GnPs and CB nanoparticles show viscoelastic near 0.4 rad s^{-1} and glass state around 100 rad s^{-1}, at which their tan δ changes significantly, Figure 10. However, the tan δ of 5.0 wt% PP/CNFs and PP/CNTs PNCs is relatively low, and the peaks are observed in their tan δ vs. ω plots between 15–25 rad s^{-1}. The delay of the tan δ as a function of ω is due to the steric hindrance of the CNFs and CNTs on the polymer chains.[6] This is attributed to the fact that the interactions among PP/CNT, PP/CNF are stronger than the PP molecules, PP/GnP, and PP/CB interaction.

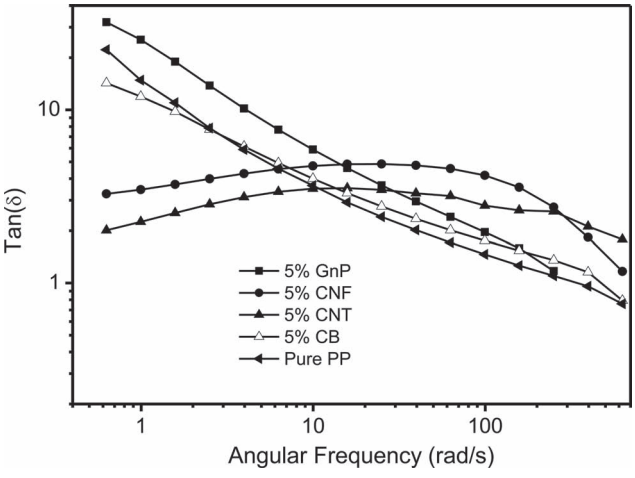

Figure 11. Mechanical loss factor (tan δ) of PP/GnP nanocomposites with different GnP loading.

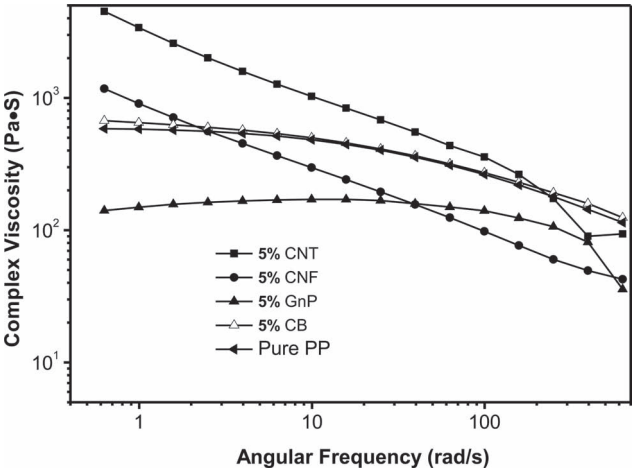

Figure 12. Complex viscosity (η^*) versus ω for pure PP and its carbon nanofiller PNCs.

The viscosity of pure PP and its PNC melts is also illustrated in a log–log scale plot of viscosity versus ω. A horizontal line indicates a Newtonian fluid and the decreased viscosity with increasing shear rate or ω is defined as shear thinning.[59,60] Figure 12 shows the complex viscosity (η^*) of neat PP and its 5.0 wt% carbon nanofiller PNC melts. η^* is observed to decrease with increasing ω, indicating that neat PP and its PNCs exhibit a typical shear thinning behavior. η^* of these PNC melts is 149 Pa s, 589, 670, 920, 3498 Pa s for 5.0 wt% PP/GnP, pure PP, 5.0 wt% PP/CB, 5.0 wt% PP/CNF, and 5.0 wt% PP/CNT PNCs, respectively. The increment of the melt viscosity results from the strong interaction between CNFs, CNTs, and PP chains, which restricts the PP chain movements more significantly, especially at low ω. Many carbon nanofillers, such as SWCNTs and metal oxide nanoparticles, have also been reported to be able to interact strongly with the polymer matrix and cause an elevated η^*.[59,60] However, compared to that of pure PP, the PNCs with a loading of 5.0 wt% GnP have a low η^*, which is attributed to the slippage between GnPs and PP.

4. Conclusion

The PP PNCs containing different carbon nanofillers were prepared through a facile solution dispersion method. The PNCs with different geometric carbon nanofillers showed different electrical percolation thresholds. CNFs and CNTs could form a filler network in the matrix at a lower loading than CB and GnPs. As compared to neat PP, all the PNCs exhibited an improved thermal stability. The effects of different carbon nanofillers on the melt rheological behaviors were also investigated. A reduced or close storage modulus and complex viscosity were observed for the PP/GnP and PP/CB PNC melts. However, the melt rheological behaviors of 5.0 wt% PP/CNF and PP/CNT PNCs were very different from those of the PP/GnP and PP/CB PNCs with the loading over the critical percolation threshold, and an enhanced storage modulus and complex viscosity in the PNC melts were observed. The nanofiller aspect ratio has a very significant impact on the electrical conductivity, thermal stability, and melt rheological behavior of the PNCS.

Acknowledgements: The authors gratefully thank Dr. J. A. Gomes for assistance with the XRD measurements. This project is supported by the National Science Foundation-Nanoscale Interdisciplinary Research Team and Materials Processing and Manufacturing (CMMI 10-30755). S. W. acknowledges support from the Welch Foundation (V-0004).

Received: June 25, 2011; Revised: August 10, 2011; Published online: October 17, 2011; DOI: 10.1002/macp.201100364

Keywords: carbon nanostructure materials; electrical conductivity; melt rheological behavior; nanocomposites; poly(propylene) (PP)

[1] J. Zhu, S. Wei, J. Ryu, M. Budhathoki, G. Liang, Z. Guo, *J. Mater. Chem.* **2010**, *20*, 4937.
[2] K. Kalaitzidou, H. Fukushima, L. T. Drzal, *Carbon* **2007**, *45*, 1446.
[3] R. Dweiri, J. Sahari, *J. Power Sources* **2007**, *171*, 424.
[4] M. Yoonessi, J. R. Gaier, *ACS Nano* **2010**, *4*, 7211.
[5] N. Grossiord, M. E. L. Wouters, H. E. Miltner, K. Lu, J. Loos, B. V. Mele, C.E. Koning, *Eur. Polym. J.* **2010**, *46*, 1833.
[6] X. Chen, S. Wei, S. A. Yadav, R. Patil, J. Zhu, R. Ximenes, L. Sun, Z. Guo, *Macromol. Mater. Eng.* **2011**, *296*, 434.
[7] M. Xiao, L. Sun, J. Liu, Y. Li, K. Gong, *Polymer* **2002**, *43*, 2245.
[8] L. Sun, J. Y. O'Reilly, C.-W. Tien, H.-J. Sue, *J. Chem. Educ.* **2008**, *85*, 1105.
[9] J. Zhu, S. Wei, A. Yadav, Z. Guo, *Polymer* **2010**, *51*, 2643.
[10] J. Zhu, S. Wei, J. Ryu, Z. Guo, *J. Phys. Chem. C* **2011**, *115*, 13215.
[11] M. Narkis, A. Ram, Z. Stein, *Polym. Eng. Sci.* **1981**, *21*, 1049.
[12] M. Maiti, S. Sadhu, A. K. Bhowmick, *J. Appl. Polym. Sci.* **2005**, *96*, 443.
[13] M. Drubetski, A. Siegmann, M. Narkis, *J. Mater. Sci.* **2007**, *42*, 1.
[14] L. Sun, G. L. Warren, J. Y. O'Reilly, W. N. Everett, S. M. Lee, D. Davis, D. Lagoudas, H. J. Sue, *Carbon* **2008**, *46*, 320.
[15] G. L. Warren, L. Sun, V. G. Hadjiev, D. Davis, D. Lagoudas, H.-J. Sue, *J. Appl. Polym. Sci.* **2009**, *112*, 290.
[16] V. G. Hadjiev, G. L. Warren, L. Sun, D. C. Davis, D. C. Lagoudas, H. J. Sue, *Carbon* **2010**, *48*, 1750.
[17] L. Sun, G. L. Warren, H.-J. Sue, *Carbon* **2010**, *48*, 2364.
[18] L. Sun, G. Warren, D. Davis, H. J. Sue, *J. Mater. Sci.* **2011**, *46*, 207.
[19] J. C. Kearns, R. L. Shambaugh, *J. Appl. Polym. Sci.* **2002**, *86*, 2079.
[20] F. Du, R. C. Scogna, W. Zhou, S. Brand, J. E. Fischer, K. I. Winey, *Macromolecules* **2004**, *37*, 9048.
[21] T. Soitong, J. Pumchusak, *J. Appl. Polym. Sci.* **2011**, *119*, 962.

[22] K. Lozano, E. V. Barrera, *J. Appl. Polym. Sci.* **2001**, *79*, 125.
[23] H. Kim, A. A. Abdala, C. W. Macosko, *Macromolecules* **2010**, *43*, 6515.
[24] H. Kim, Y. Miura, C. W. Macosko, *Chem. Mater.* **2010**, *22*, 3441.
[25] K. Wakabayashi, P. J. Brunner, J. I. Masuda, S. A. Hewlett, J. M. Torkelson, *Polymer* **2010**, *51*, 5525.
[26] L. Sun, M. Xiao, J. Liu, K. Gong, *Eur. Polym. J.* **2006**, *42*, 259.
[27] Y. Li, J. Zhu, S. Wei, J. Ryu, L. Sun, Z. Guo, *Macromol. Chem. Phys.* **2011**, *212*, 1951.
[28] S. Wei, R. Patil, L. Sun, N. Haldolaarachchige, X. Chen, D. P. Young, Z. Guo, *Macromol. Mater. Eng.* **2011**, *296*, 850
[29] J. Zhu, S. Wei, Y. Li, L. Sun, N. Haldolaarachchige, D. P. Young, C. Southworth, A. Khasanov, Z. Luo, Z. Guo, *Macromolecules* **2011**, *44*, 4382.
[30] S. Zhang, A. R. Horrocks, *Prog. Polym. Sci.* **2003**, *28*, 1517.
[31] J. M. Keith, J. A. King, B. A. Johnson, *J. New Mater. Electrochem. Syst.* **2008**, *11*, 253.
[32] L. Sun, J. Liu, S. R. Kirumakki, E. D. Schwerdtfeger, R. J. Howell, K. Al-Bahily, S. A. Miller, A. Clearfield, H.-J. Sue, *Chem. Mater.* **2009**, *21*, 1154.
[33] A. Funck, W. Kaminsky, *Compos. Sci. Technol.* **2007**, *67*, 906.
[34] A. A. Koval'chuk, V. G. Shevchenko, A. N. Shchegolikhin, P. M. Nedorezova, A. N. Klyamkina, A. M. Aladyshev, *Macromolecules* **2008**, *41*, 7536.
[35] F. Salaün, I. Vroman, G. Bedek, M. Lewandowski, *J. Polym. Sci., Part B: Polym. Phys.* **2008**, *46*, 2566.
[36] L. S. Montagna, F. d. C. Fim, G. B. Galland, N. R. d. S. Basso, *Macromol. Symp.* **2011**, *299,* 48.
[37] Z. Zhou, S. Wang, Y. Zhang, Y. Zhang, *J. Appl. Polym. Sci.* **2006**, *102*, 4823.
[38] P. Morgan, *Carbon Fiber and Their Composites*, Taylor & Francis Group, Boca Raton, FL **2005**.
[39] J. A. King, B. A. Johnson, M. D. Via, C. J. Ciarkowski, *J. Appl. Polym. Sci.* **2009**, *112*, 425.
[40] G. Heinrich, T. A. Vilgis, *Macromolecules* **1993**, *26*, 1109.
[41] F. Gubbels, R. Jerome, P. Teyssie, E. Vanlathem, R. Deltour, A. Calderone, V. Parente, J. L. Bredas, *Macromolecules* **1994**, *27*, 1972.
[42] J. Z. Liang, Q. Q. Yang, *J. Reinf. Plast. Compos.* **2009**, *28*, 295.
[43] B. J. P. Adohi, A. Mdarhri, C. Prunier, B. Haidar, C. Brosseau, *J. Appl. Phys.* **2010**, *108*, 074108.
[44] M. Moniruzzaman, K. I. Winey, *Macromolecules* **2006**, *39*, 5194.
[45] J. R. Potts, D. R. Dreyer, C. W. Bielawski, R. S. Ruoff, *Polymer* **2011**, *52*, 5.
[46] I. Balberg, *Carbon* **2002**, *40*, 139.
[47] E. T. Thostenson, C. Li, T.-W. Chou, *Compos. Sci. Technol.* **2005**, *65*, 491.
[48] J. H. Lee, Y. K. Jang, C. E. Hong, N. H. Kim, P. Li, H. K. Lee, *J. Power Sources* **2009**, *193*, 523.
[49] G. Chen, W. Zhao, in *Nano- and Biocomposites*, (Eds: A. K.-T. Lau, F. Hussain, K. Lafdi), CRC Press, Boca Raton, FL **2010**.
[50] *Handbook of Low and High Dielectric Constant Materials and Their Applications (2 Vol. Set)*, (Ed: H. S. Nalwa), Academic Press, New York **1999**.
[51] Z. M. Dang, L. Wang, Y. Yin, Q. Zhang, Q. Q. Lei, *Adv. Mater.* **2007**, *19*, 852.
[52] T. Nishino, T. Matsumoto, K. Nakamae, *Polym. Eng. Sci.* **2000**, *40*, 336.
[53] G. Machado, E. L. G. Denardin, E. J. Kinast, M. C. Gonçalves, M. A. de Luca, S. R. Teixeira, D. Samios, *Eur. Polym. J.* **2005**, *41*, 129.
[54] D. V. Talapin, S. Haubold, A. L. Rogach, A. Kornowski, M. Haase, H. Weller, *J. Phys. Chem. B* **2001**, *105*, 2260.
[55] T. V. Monakhova, P. M. Nedorezova, T. A. Bogayevskaya, V. I. Tsvetkova, Y. A. Shlyapnikov, *Polym. Sci. USSR* **1988**, *30*, 2589.
[56] A. Chatterjee, B. L. Deopura, *J. Appl. Polym. Sci.* **2006**, *100*, 3574.
[57] Q. Yuan, R. D. K. Misra, *Polymer* **2006**, *47*, 4421.
[58] D. Wu, Y. Sun, L. Wu, M. Zhang, *J. Appl. Polym. Sci.* **2008**, *108*, 1506.
[59] J. D. Ferry, *Viscoelastic Properties of Polymers*, 3rd ed, Wiley, New York **1980**.
[60] J. A. King, M. D. Via, J. M. Keith, F. A. Morrison, *J. Compos. Mater.* **2009**, *43*, 3073.